

# A Lagrangian Analysis of Water Vapor Sources and Pathways for Precipitation in East China in Different Stages of the East Asian Summer Monsoon

YI SHI AND ZHIHONG JIANG

*Key Laboratory of Meteorological Disaster of Ministry of Education, Collaborative Innovation Center on Forecast and Evaluation of Meteorological Disasters, Nanjing University of Information Science and Technology, Nanjing, China*

ZHENGYU LIU

*Atmospheric Science Program, Department of Geography, The Ohio State University, Columbus, Ohio*

LAURENT LI

*Laboratoire de Météorologie Dynamique, CNRS, Sorbonne Université, Ecole Normale Supérieure, Ecole Polytechnique, Paris, France*

(Manuscript received 31 January 2019, in final form 23 October 2019)

## ABSTRACT

The Hybrid Single-Particle Lagrangian Integrated Trajectory (HYSPPLIT) platform is used to simulate Lagrangian trajectories of air parcels in East China during the summer monsoon. The investigation includes four distinct stages of the East Asian summer monsoon (EASM) during its seasonal migration from south to north. Correspondingly, the main water vapor channel migrates from the west Pacific Ocean (PO) for the premonsoon in South China (SC) to the Indian Ocean (IO) for the monsoon in SC and in the Yangtze–Huaihe River basin, and finally back to the PO for the terminal stage of monsoon in North China. Further calculations permit us to determine water vapor source regions and water vapor contribution to precipitation in East China. To a large extent, moisture leading to precipitation does not come from the strongest water vapor pathways. For example, the proportions of trajectories from the IO are larger than 25% all of the time, but moisture contributions to actual precipitation are smaller than 10%. This can be explained by the large amount of water vapor lost in the pathways across moisture-losing areas such as the Indian and Indochina Peninsulas. Local water vapor recycling inside East China (EC) contributes significantly to regional precipitation, with contributions mostly over 30%, although the trajectory proportions from subregions in EC are all under 10%. This contribution rate can even exceed 55% for the terminal stage of the monsoon in North China. Such a result provides important guidance to understand the role of land surface conditions in modulating rainfall in North China.

## 1. Introduction

Unlike tropical summer monsoons, such as the Indian monsoon or the West African monsoon, the East Asian summer monsoon (EASM) is characterized by the presence of a front between warm air masses from the south and cold air masses from the north (Wang 2006;

Chang 2004). A rain belt is formed along the front. During the seasonal course in summer, the rain belt marks a clear migration from south to north, making different rainy periods in different regions in East China. It is well recognized that three major periods of rainfall take place in South China, the Yangtze River basin, and North China (Zhou and Yu 2005; Ding et al. 2008; Shi et al. 2009; Sun et al. 2011; Zhu et al. 2011; Sun and Wang 2015). The rain belt, whatever its geographic position during its migration course from south to north, is always strongly related to moisture transport, which is a necessary condition leading to precipitation (Huang et al. 1998; Jiang et al. 2006; Sun et al. 2011). It

---

Supplemental information related to this paper is available at the Journals Online website: <https://doi.org/10.1175/JCLI-D-19-0089.s1>.

---

Corresponding author: Zhi-Hong Jiang, zhjiang@nuist.edu.cn

DOI: 10.1175/JCLI-D-19-0089.1

© 2020 American Meteorological Society. For information regarding reuse of this content and general copyright information, consult the [AMS Copyright Policy](#) ([www.ametsoc.org/PUBSReuseLicenses](http://www.ametsoc.org/PUBSReuseLicenses)).

is of great significance to quantitatively determine the moisture source of the monsoon rainfall for its different phases.

Early research mainly used an Eulerian approach to analyze moisture transport pathways. For the rainy period in South China, [Lin et al. \(2014\)](#) showed that southwesterly water vapor transports carrying moisture from the Bay of Bengal, the west Pacific, and the southwest side of the Tibetan Plateau are major pathways. For the mei-yu rainy season in the Yangtze River Valley, [Jiang et al. \(2009\)](#) showed that water vapor is mainly from the southern Indian Ocean, the East African coast, and the Arabian Sea. For rainfall in North China, [Xie and Ren \(2008\)](#) indicated that water vapor mainly comes from the Bay of Bengal, the South China Sea/west Pacific Ocean, and the midlatitude westerlies. These research studies mainly focused on the moisture transport channels during the EASM, and indicated the significant changes for different stages of the summer monsoon.

However, the simple analysis of moisture transport with an Eulerian vision is unable to assess moisture origins from remote regions. It generally ignores any moisture changes during the transport, although some Eulerian variants with an online implementation of moisture tagging technique in global or regional climate models were proved to be very useful to understand water vapor sources [see [Insua-Costa and Miguez-Macho \(2018\)](#) and the relevant references there]. When such a water vapor tracer scheme was incorporated into the regional model WRF, [Dominguez et al. \(2016\)](#) and [Eiras-Barca et al. \(2017\)](#) were able to investigate the origin of moisture for the North American monsoon and for two events of atmospheric river landfall causing catastrophic precipitation.

The most advanced methods that have been widely used in recent years to determine moisture origin are based on Lagrangian models ([Stohl and James 2004, 2005](#); [Dominguez et al. 2006](#); [Dirmeier et al. 2009](#)), capable of calculating backward or forward trajectories of air parcels residing over the target region. They can trace pathways of the moisture transport and changes of physical quantities along the pathways. The Lagrangian methodology has been highly valued in investigating global moisture transport and regional moisture recycling. We can cite a few works to show the diversity of research topics that used the Lagrangian approach. First, at the global scale, [Gimeno et al. \(2010\)](#) presented results on the moisture contribution for each continent from the global ocean in different seasons. At the regional scale, [Brubaker et al. \(2001\)](#) and [Diem and Brown \(2006\)](#) calculated the moisture sources for precipitation in the Mississippi River basin and in the southwestern United States. [Bertò et al. \(2004\)](#), [Perry et al. \(2007\)](#), [Sodemann and Stohl \(2009\)](#), and [Bottyán et al. \(2014\)](#) demonstrated that water vapor

for rainfall in southern Europe comes, in large part, from the Mediterranean Sea.

For East China, there have also been numerous studies using Lagrangian models. [Drumond et al. \(2011a\)](#) revealed the main moisture source in different regions in China. [Sun and Wang \(2014, 2015\)](#) detected the origins of moisture over East China and semiarid grassland. However, different researches are still quite divergent. [Chen et al. \(2013\)](#) showed that the moisture of summer rainfall in the Yangtze–Huaihe River basin is mainly from the South China Sea and the Bay of Bengal. [Drumond et al. \(2011a\)](#) indicated that the moisture of East China is mainly from the East China Sea, and the moisture of South China is mainly from the Bay of Bengal and the Arabian Sea. In recent work, [Sun and Wang \(2015\)](#) affirmed that the water vapor for precipitation in the Yangtze–Huaihe River basin and in North China is mainly from local evaporation and from the west Pacific Ocean.

The divergence of results in the scientific literature has two major sources. First, the target area in East China is different among different publications. There has been a lack of systematic investigation for different regions and for the whole seasonal course when the East Asian summer monsoon migrates from south to north. Second, since the calculations of Lagrangian trajectories require heavy computation, many existing studies have been limited to short periods, which may impact the stability and robustness of their results. It is thus desirable to study different phases during the seasonal migration course of the rainfall in East China for a long time period.

In this article, based on the Hybrid Single-Particle Lagrangian Integrated Trajectory (HYSPPLIT) platform of Lagrangian trajectories, we systematically analyze the variation of water vapor transport in East China during different phases of EASM. Our analysis covers the period from 1961 to 2010. Advanced diagnostics are performed to assess moisture transport pathways, moisture sources, and contributions to precipitation in each phase of EASM.

The article is organized as follows: the data and analyzing methods are described in [section 2](#). [Section 3](#) presents the main results on the water vapor sources and contributions from different regions during the northward propagation of EASM. It furthermore quantifies the proportion of trajectories and the contribution of water vapor to precipitation during the seasonal course of EASM. Conclusions are drawn in the last section.

## 2. Data and methods

### a. Data

We used the reanalysis data taken from the National Centers for Environmental Prediction (NCEP)–National

Center for Atmospheric Research (NCAR) reanalysis. Global pressure-level data were reprocessed into the HYSPLIT compatible format in the Air Resources Laboratory (ARL) of the National Oceanic and Atmospheric Administration (NOAA). They are available since 1948 at 6-hourly temporal resolution and  $2.5^\circ$  (latitude/longitude grid) spatial resolution with 17 levels in the vertical. Data have been downloaded from the ARL's archives ([http://ready.arl.noaa.gov/gbl\\_reanalysis.php](http://ready.arl.noaa.gov/gbl_reanalysis.php)).

### b. Determination of the rainy season course in East China

The rainy season course in East China is directly taken from the *National Climate Bulletin* published annually by the National Climate Center and the Central Meteorological Observatory (<http://cmdp.ncc-cma.net/cn/monitoring.htm#>). As commonly practiced (Jiang et al. 2006; Sun and Wang 2014, 2015; Zhou and Yu 2005; Ding et al. 2008), the rainy season course in East China is divided into three periods and characterized by abundant rainfall in three geographical regions which are, from south to north, South China (SC), the Yangtze–Huaihe River (YHR) basin, and North China (NC). The data period covers from 1961 to 2010. The three areas are shown in Fig. 1 with the following coordinates:  $20^\circ$ – $26^\circ$ N,  $106^\circ$ – $120^\circ$ E;  $28^\circ$ – $34^\circ$ N,  $110^\circ$ – $123^\circ$ E; and  $35^\circ$ – $43^\circ$ N,  $110^\circ$ – $120^\circ$ E, respectively.

The situation in SC can be divided into two distinct subperiods separated by the onset of the South China Sea (SCS) summer monsoon, which induces different characteristics of atmospheric circulation in South China and associated water vapor transport (Shen et al. 1982; Chen et al. 1991; Lin et al. 2014). Before the onset of SCS summer monsoon, the water vapor transport in South China is associated with the westerly wind belt and SCS sea level pressure high. With the onset and strengthening of the SCS monsoon, the cross-equatorial flow from the Southern Hemisphere intensifies and connects with the water vapor channel from the Bay of Bengal. Regarding the onset date of the SCS monsoon, we use that defined by Wang et al. (2004), namely the day when the 850-hPa zonal winds averaged over the central SCS ( $5^\circ$ – $15^\circ$ N,  $110^\circ$ – $120^\circ$ E) shift from westerlies to easterlies. Figure 2 shows the beginning and ending dates of the four periods characterizing the rainy season course of East China from 1961 to 2010. The average start days of the four periods are 6 April, 17 May, 8 June, and 16 July. The average end days are 16 May, 1 June, 17 July, and 18 August. As shown in Fig. 2, there is a large interannual variability for the timing and duration of these four subperiods, which obligates us to use precise beginning and end dates in our statistics of trajectories.

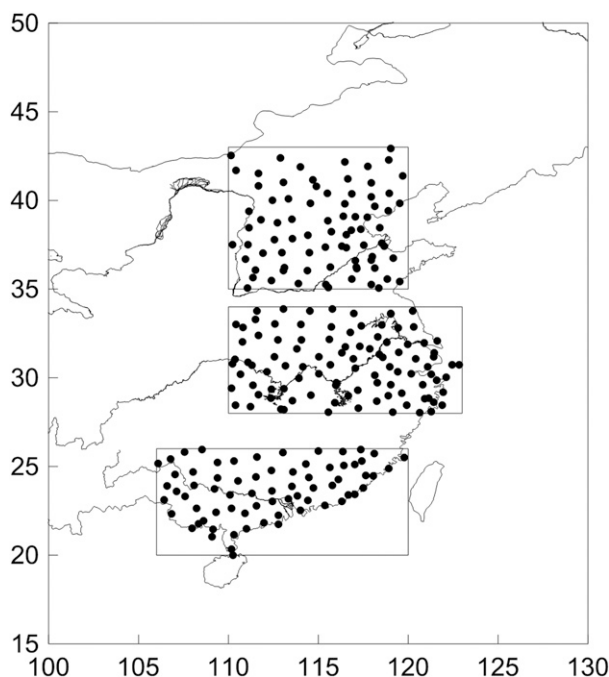


FIG. 1. Location of the three rectangular target domains in East China, the North China region ( $35^\circ$ – $43^\circ$ N,  $110^\circ$ – $120^\circ$ E), Yangtze–Huaihe River basin region ( $28^\circ$ – $34^\circ$ N,  $110^\circ$ – $123^\circ$ E), and South China region ( $20^\circ$ – $26^\circ$ N,  $106^\circ$ – $120^\circ$ E) from north to south. Dots indicate locations of the observational stations in these three regions. Superimposed are three major rivers in East China: the Pearl River in the south, the Yangtze River in the middle, and the Yellow River in the north.

### c. Methods

#### 1) HYSPLIT WATER VAPOR TRACKING SIMULATION

The NOAA HYSPLIT model (Draxler and Hess 1998; NOAA ARL 2011) is used in this paper for trajectories and tracks of air parcels. The back-trajectory algorithm is applied to all stations inside the three target areas. From their initial position, back trajectories are calculated to cover all times between the beginning and the end of each of the four subperiods of the monsoon propagation course. We use six levels at 100, 500, 1500, 3000, 5000, and 9000 m as our initial height of particle release. These levels roughly correspond to the near-surface layer and levels at 925, 850, 700, 500, and 300 hPa, respectively. All parcels were integrated backward in time, until 10 days. Outputs were recorded every 6 h with variables indicating the position (latitude, longitude, and altitude) and meteorological conditions (temperature, specific humidity, and geopotential height) for further analysis and diagnostics (Jiang et al. 2017). In particular, we averaged all trajectories in each of the five main moisture source areas, which helps us to get actual moisture transport pathways.

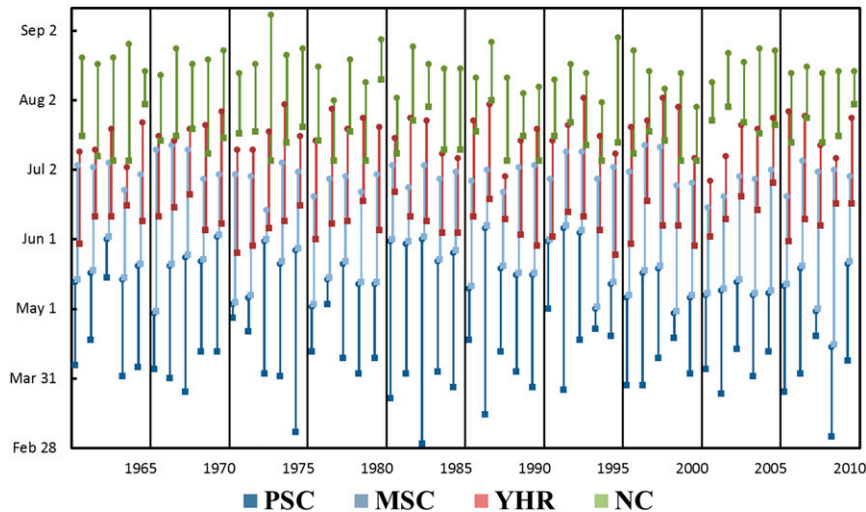


FIG. 2. Beginning and end dates of the premonsoon in South China (PSC; dark blue), monsoon in South China (MSC; light blue), monsoon (or mei-yu) in the Yangtze-Huaihe River basin (YHR; red), and monsoon in North China (NC; green) from 1961 to 2010.

## 2) EVAPORATION-MINUS-PRECIPITATION DIAGNOSIS METHOD ( $E - P$ ) TO DEDUCE SOURCE/SINK REGIONS OF WATER VAPOR

Water vapor in an air parcel changes when evaporation or precipitation takes place, increasing with the former and decreasing with the latter. It is thus clear that a correct determination of the source and sink characteristics of the water vapor transport has to take into account processes of evaporation and precipitation following the trajectory. [Stohl and James \(2004, 2005\)](#) proposed such a diagnostic method, commonly called the evaporation-minus-precipitation method, to consider the change of moisture content with time as the air parcel travels. The budget equation can be written as follows:

$$e - p = m \frac{dq}{dt}, \quad (1)$$

where  $e$  and  $p$  are respectively the rates of evaporation and precipitation,  $q$  is the specific humidity, and  $m$  is the mass of the air parcel. For a given air parcel, when  $q$  decreases, precipitation is larger than evaporation, and the parcel loses water vapor. When  $q$  increases, evaporation is larger than precipitation, and the parcel gains water vapor. Summing the  $e - p$  of all air parcels residing in the atmospheric column over an area  $A$ , the surface net water flux in the area can be given by the following equation:

$$E - P \approx \frac{\sum_{k=1}^K (e - p)}{A}, \quad (2)$$

where  $E$  and  $P$  are the total evaporation and precipitation in the column and  $K$  is the number of particles

over the area. Equation (2) can be regarded as a Lagrangian transformation of the Eulerian atmospheric moisture budget equation:

$$E - P = \frac{\partial W}{\partial t} + \nabla \cdot \frac{1}{g} \int_0^{P_s} q \mathbf{v} dp, \quad (3)$$

where  $W = (1/g) \int_0^{P_s} q dp$  is the vertically integrated water vapor or precipitable water in the column,  $g$  is the gravitational acceleration,  $\mathbf{v}$  is wind,  $p$  is atmospheric pressure, and  $P_s$  is pressure at the surface. The last term in Eq. (3) represents the divergence of vertically integrated water vapor flux. [Stohl and James \(2004, 2005\)](#) showed that when using a large enough number of particles, the Lagrangian and Eulerian methods give almost identical results. So the  $E - P$  results can be obtained, and the overall water vapor budget in a certain region can be further determined. The case  $E - P > 0$  indicates that the area is source of water vapor to the precipitation in target region, whereas when  $E - P < 0$  the area is a sink to the precipitation to the target region. More details of this evaporation-minus-precipitation method can be found in [Stohl and James \(2004, 2005\)](#) and [Sodemann and Zubler \(2010\)](#).

## 3) THE IMPROVED AREAL SOURCE-RECEPTOR ATTRIBUTION METHOD

The evaporation-minus-precipitation diagnosis can be used to determine the regional source and sink characteristics of the water vapor, but it cannot quantify the composition of actual contribution of various water vapor sources to the precipitation in the considered area. For example, a region of high positive

evaporation-minus-precipitation value can almost certainly be considered as a moisture source region. However, the air parcels passing over this region to a target region may not carry a large amount of moisture from this source region into the target region. This issue of water vapor contribution from a source point to a target point can be assessed if one performs a further simple (forward) operation on the identified trajectories with a consideration of water vapor evolution (evaporation and precipitation) along the trajectories. Sodemann et al. (2008) and Martius et al. (2013) reported interesting results about moisture source attribution within this simple framework.

However, this attribution calculation is only valid from a source point to a target point. It fails when one wants to evaluate an area for either the source or the target (or both). As a remedy of this drawback, Sun and Wang (2014) introduced a method called the areal source–receptor attribution to evaluate the contribution of a specific water vapor source region to the precipitation in a target region. When the air parcel is between the source and target regions, a normal operation is applied to calculate water vapor changes in function of evaporation (precipitation) that increases (decreases) water vapor. The specificity of the areal source–receptor attribution method is in its special treatments when the air parcel is in the source and target regions. Details can be found in step 5 of the algorithm, which is decomposed into seven steps and presented in Sun and Wang (2014).

In our study, we further improve the methodology with two new aspects. First, we take into account the water vapor in the initial air parcels (when the back trajectories reach a level below 50 m and cannot go farther), while Sun and Wang (2014) put this initial water vapor content at zero. This enhances the overall contribution rate of water vapor. Second, as also suggested in Huang et al. (2018), we consider a gain of water vapor when parcels flow below the boundary layer top, where vertical mixing is dominant. Air parcels in this case are considered to be gaining water vapor as from the ground, while an increase of specific humidity above the boundary layer is mainly affected by a phase change of water vapor. In the latter case, we cannot directly assign the region as a source region.

A third improvement that we implemented in the initial algorithm of Sun and Wang (2014) is consideration of the source region. The initial algorithm took into account only a well-determined source/target duality. In our work here, we extend the source region to an ensemble of unit surface areas of  $1^\circ \times 1^\circ$  latitude/longitude. This permits us to introduce the concept of the contribution density function (CDF), while Sun and Wang (2014) could calculate only the contribution proportion from source to target.

To summarize, we can now calculate, for each trajectory  $j$  departing from the grid  $i$ , the quantity  $R_j(i)$  representing the moisture gained from the unit surface area  $i$  and then released in the target region. Let  $R_{\text{total}}$  be the precipitation falling down in the target. It should be the general sum of  $R_j(i)$ , that is, the total moisture release from all trajectories (Sodemann et al. 2008; Sun and Wang 2014, 2015; Chu et al. 2017). But it is actually a little larger than the general sum, due to the lack of trajectory calculations at very high layers. The contribution of water vapor from each unit area can be assessed with the contribution density function, defined and calculated as

$$\text{CDF}(i) = \frac{\sum_{j=1}^n R_j(i)}{R_{\text{total}}}, \quad (4)$$

where  $n$  is the number of trajectories departing from the area  $i$ . CDF behaving as a 2D probability density function can serve as a measure to evaluate the moisture contribution rate of a unit area  $i$  to the precipitation falling into the target area.

With the improvement that we implemented, the global integration of CDF is significantly increased, which indicates that we can more accurately identify water vapor sources for the precipitation. For example, the global sum of CDF for North China monsoon rainfall is about 0.8 with the original method (Sun and Wang 2015), and about 0.9 with our modifications.

### 3. Results

Based on the methodology described in section 2c, we simulated the backward trajectory of parcels for EASM. From their initial positions shown in Fig. 1, back-trajectories are calculated to cover all times during the four subperiods of monsoon propagation in Fig. 2 for 10 days.

#### a. Premonsoon in South China

For the premonsoon, rainfall mainly occurs in South China. Although it is before the onset of the SCS summer monsoon, rainfall is still considered as part of EASM. We first analyze the moisture transport pathways (or channels) obtained as the mean trajectory, which is the average of all back trajectories departing from our predefined geographic sectors. Figure 3a shows the main water vapor transport pathways (or channels) during the premonsoon in South China. The trajectory proportions are also shown in relation to the channels. For the premonsoon in South China, the most important water vapor transport channel is from the west Pacific Ocean, accounting for 33.3% of all trajectories. Air parcels come from the west Pacific

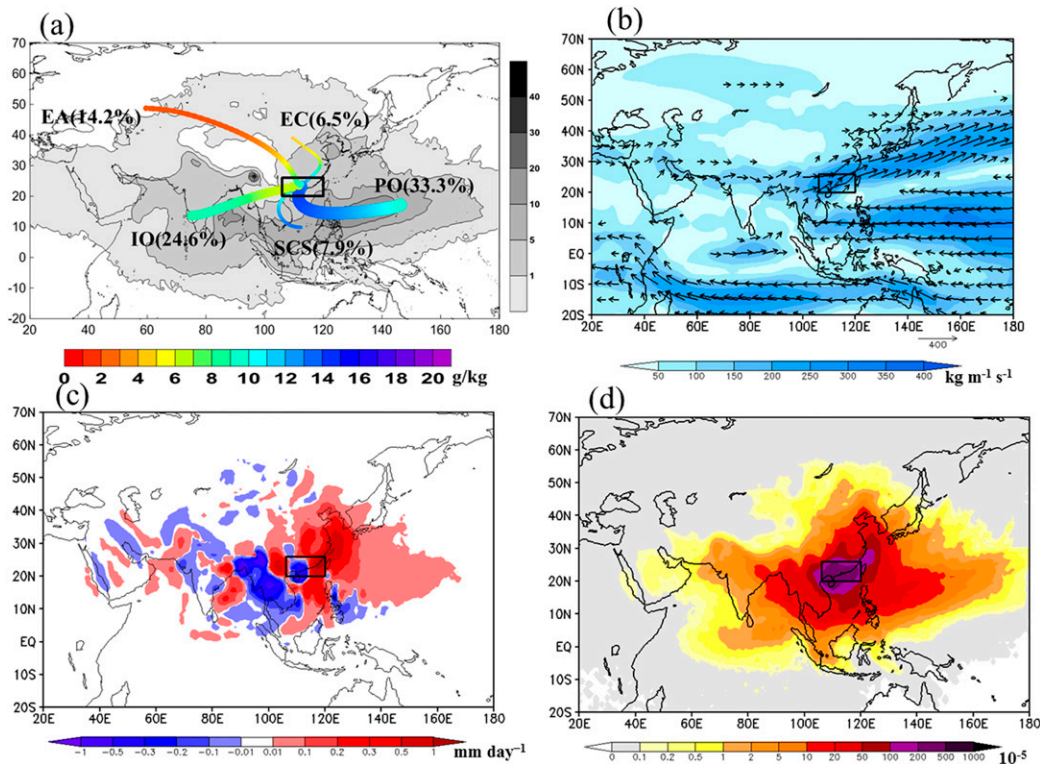


FIG. 3. Characteristics of moisture transport and moisture source and sink for the premonsoon in South China (SC). (a) Moisture transport channels based on average trajectories. Five transport channels are identified, from East China (EC), the west Pacific Ocean (PO), the South China Sea (SCS), the Indian Ocean (IO), and the Eurasian westerly (EA), respectively. Colors on the pathways indicate the average specific humidity of air parcels along the trajectories ( $\text{g kg}^{-1}$ ). The thickness of the pathways represents the percentage of trajectories, also indicated in numbers. Gray shadings are the number of particles weighted by specific humidity ( $\text{g kg}^{-1}$ ) arriving in the target region (the rectangular zone) for day 10. (b) The climatology of vertically integrated atmospheric water vapor transport (vectors;  $\text{kg m}^{-1} \text{s}^{-1}$ ) under the Eulerian view; only vectors more than  $50 \text{ kg m}^{-1} \text{s}^{-1}$  are shown, and shadings represent the amount of the water vapor transport. (c) Mean  $E - P$  ( $\text{mm day}^{-1}$ ) of air parcels in 1–10 days before reaching target region (the rectangular zone). (d) Water vapor contribution density function (CDF) showing the contribution of water vapor source regions ( $10^{-5}$ ; areas of  $1^\circ \times 1^\circ$  in latitude/longitude) to the precipitation in the target region of South China.

Ocean, move northwestward across the Philippines, and finally enter the target area at the south boundaries. The average specific humidity of air parcels increases from  $10$  to  $14 \text{ g kg}^{-1}$ , which indicates that a significant portion of moisture is absorbed along the trajectories. The secondary moisture transport channel is from the Indian Ocean, which accounts for 24.6% of all trajectories. The average trajectories move across the Bay of Bengal and the Indochina Peninsula and then move into South China. Contrary to the west Pacific channel, the average specific humidity of air parcels from the Indian Ocean decreases from  $12$  to  $8 \text{ g kg}^{-1}$ , which indicates a great deal of water vapor loss. Of the trajectories, 14.2% are from the westerlies in the north, and their average specific humidity is small, increasing from  $2$  to  $7 \text{ g kg}^{-1}$ . Besides, the proportion of local trajectories is 6.5% and the South

China Sea channel accounts for about 7.9% and the average specific humidity is  $14 \text{ g kg}^{-1}$ , the largest among all the channels. These results are consistent with our general expectation, and in agreement with Chen and Luo (2018), who also concluded that the main water vapor transport channel during the premonsoon period in South China is from the Pacific Ocean. Nevertheless, the trajectory proportion obtained from our research is a bit higher for the Pacific Ocean and lower for the South China Sea.

The vertically integrated water vapor transports within the Eulerian framework are shown in Fig. 3b. The premonsoon in South China is mainly influenced by the west Pacific moisture transport channel. The circulation from southeast over the west Pacific carries abundant water vapor into the Indochina Peninsula and then affects South China. Compared to the water

vapor channel from the west Pacific Ocean, the one from the Indian Ocean is relatively weak, but it also plays an important role for the premonsoon in South China. These results are consistent with the existing literature for this regard. For example, [Chi et al. \(2005\)](#) and [Lin et al. \(2014\)](#) showed already that before the onset of SCS summer monsoon, the subtropical high dominates the South China Sea and moisture reaching South China mainly comes from west winds over the Arabian Sea, east winds at the southwest flank of the western Pacific subtropical high, and southwest winds over the Bay of Bengal.

However, the transport pathways cannot give precise moisture source/sink characteristics. Based on the evaporation-minus-precipitation diagnosis, [Fig. 3c](#) shows the spatial distribution of average  $E - P$  from 1 to 10 days before air parcels reaching South China. It clearly reveals that the west Pacific is the most important moisture source region for the premonsoon in South China, and the maximum value is located in offshore areas of East China. East China and the South China Sea are also important moisture source regions. The moisture sink region for the precipitation in South China is mainly in the Indochina Peninsula, which indicates great moisture loss from the Indian Ocean.

The spatial distribution of moisture contribution leading to premonsoon precipitation in South China (water vapor CDF) is shown in [Fig. 3d](#), obtained from the improved areal source–receptor attribution calculation. Large contribution density values are mainly located near the coasts of Southeast China, and the adjacent seas, with an average contribution density of about  $2 \times 10^{-3}$ . In the west Pacific Ocean, the CDF of  $1.0 \times 10^{-5}$  extends to  $170^\circ\text{E}$ , and that of  $1.0 \times 10^{-4}$  extends to  $150^\circ\text{E}$ . However, the CDF in the Indian Ocean monsoon region is relatively small; only the Bay of Bengal, the Indian subcontinent, and the Indochina Peninsula show CDF values larger than  $1.0 \times 10^{-5}$ .

In summary, for the premonsoon in South China, the main moisture transport channel originates from the west Pacific, which is consistent with previous work of [Chen and Luo \(2018\)](#). The most important moisture source is also from the west Pacific, providing abundant water vapor that is actually converted to precipitation in South China.

### *b. Monsoon in South China*

After the onset of SCS summer monsoon, the entire regional atmospheric circulation jumps to a new state, and EASM actually starts and enters into a stronger period. But the main monsoonal precipitation remains in South China. The main moisture transport channels are shown in [Fig. 4](#). EASM is remarkably different

from what it is in the preceding period. We can see, in [Fig. 4a](#), that the Indian Ocean moisture channel becomes the strongest one. The trajectory proportion increases from 24.6% (before the onset of SCS summer monsoon) to 53.9%. More than half of the trajectories come from the Indian Ocean. The average specific humidity increases from 10 to  $14 \text{ g kg}^{-1}$ , which also indicates that water vapor for this period is mainly from the Indian Ocean. At the same time, the west Pacific Ocean shows an obviously weaker contribution. Only 22.0% of the trajectories come from the west Pacific Ocean and the corresponding pathway is a bit northward shifted, compared to the former period. Besides, trajectories from the westerlies and from local areas are also weakened; their trajectory proportions are only 6.5% and 4.9% respectively. These results are also consistent with previous works of [Chen and Luo \(2018\)](#) and [Chu et al. \(2017\)](#). They divided the Indian Ocean channel into two channels and the sum of these two channels makes the total trajectory proportion at a level of about 50%, which is very close to our result. The vertically integrated water vapor transport, calculated within the Eulerian framework, confirms the conclusion ([Fig. 4b](#)). During this period, the southwest monsoonal flow from the Indian Ocean strengthens rapidly and the whole South Asian monsoon system goes quickly into its mature stage, with a strong Somali cross-equatorial flow, and monsoonal flows over the Arabian Sea, the Indian Peninsula, the Bay of Bengal, and the Indochina Peninsula, and finally over the South China Sea. This monsoonal flow inducing rainfall in South China is now the main moisture channel. The west Pacific Ocean channel is rapidly weakened and its influence is reduced. Such behaviors are in total agreement with what is described in the current literature (e.g., [Chi et al. 2005](#); [Lin et al. \(2014\)](#), among many others), which also shows that after the onset of SCS summer monsoon, the subtropical high withdraws out of the South China Sea, and the powerful cross-equatorial flow crosses the Bay of Bengal and transports moisture toward South China. Thus, the Indian Ocean channel is the most important moisture transport pathway in this stage.

The spatial distribution of  $E - P$  is also calculated and shown in [Fig. 4c](#). We can see that after the onset of SCS summer monsoon, the maximum value of  $E - P$  is in the northern part of the South China Sea; the moisture source from the Indian Ocean is stronger and that from the Pacific Ocean is weaker. As for moisture CDF ([Fig. 4d](#)), the biggest value is in South China and the northern part of the South China Sea where the CDF value is larger than  $2.0 \times 10^{-3}$ . The CDF in the South China Sea is about  $5.0 \times 10^{-4}$ . Compared to the rainy

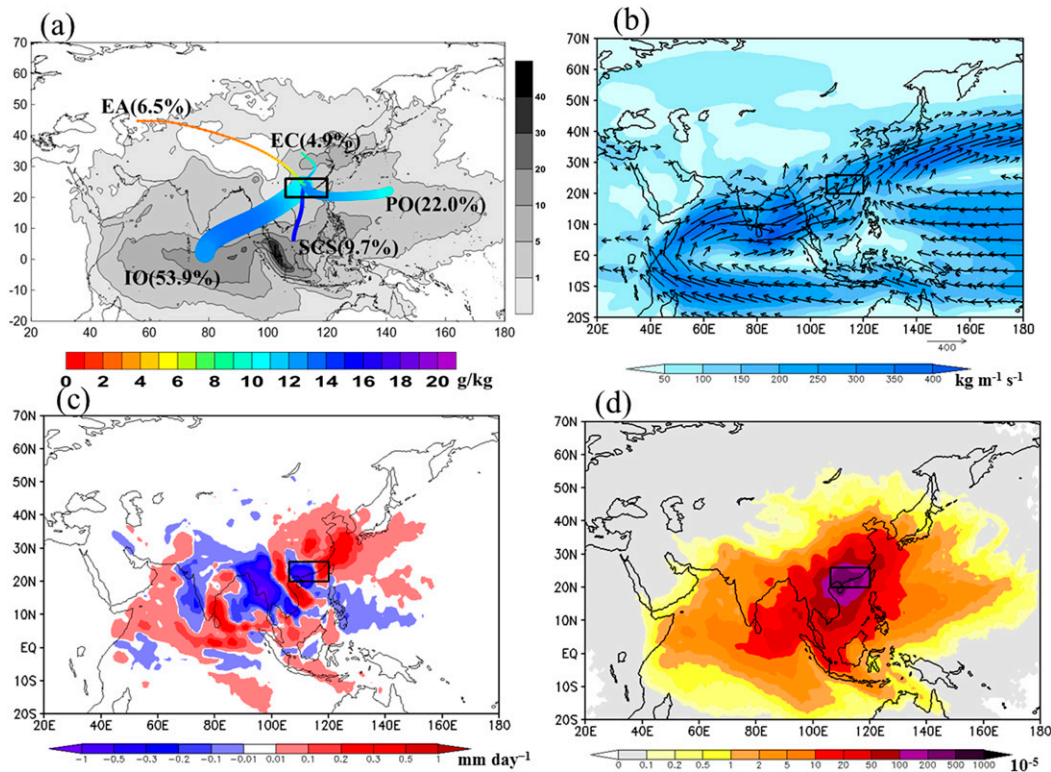


FIG. 4. As in Fig. 3, but for the starting phase of the monsoon in South China.

season before the onset of SCS summer monsoon, intensity of the CDF is decreased in the west Pacific Ocean. CDF contours of  $1.0 \times 10^{-5}$  and  $1.0 \times 10^{-4}$  extend to  $165^\circ$  and  $135^\circ\text{E}$ , respectively. This shows a clear westward shift. On the contrary, the CDF in the Indian Ocean is obviously increased. CDF values for most part of the Indian Ocean are larger than  $1.0 \times 10^{-5}$ ; CDF in the Bay of Bengal is larger than  $1.0 \times 10^{-4}$ .

During the monsoon in South China, the Indian Ocean channel is the most important moisture transport channel, which includes more than half of the trajectories, and the contribution rate also increases a lot. Meanwhile the west Pacific Ocean impact is reduced. Besides, the biggest value of the moisture contribution is in South China and the northern part of the South China Sea.

### c. Monsoon (*mei-yu*) in the Yangtze–Huaihe River basin

For the *mei-yu* period, the EASM propagates to the Yangtze–Huaihe River basin and leads to persistent rainfalls in this region. The moisture transport characters for this period have both similarities and differences with the former monsoon stage. During *mei-yu*, the IO channel is still the most important one and the portion of

trajectories reaches to 42.1%. The PO channel (22.7%) and westerly channel (13.5%) are a bit strengthening. The spatial distribution of the vertically integrated water vapor transport (Fig. 5b) shows that the IO channel, the SCS channel, and the PO channel converge in South China and move northward to converge in the Yangtze–Huaihe River basin region, resulting in plume rain in this period. Xu et al. (2004, 2008), Zuo et al. (2009), Wei et al. (2012), and Jiang et al. (2013) also indicate that the IO channel is the most important water vapor channel in the Yangtze–Huaihe River basin.

The spatial distribution of  $E - P$  (Fig. 5c) also shows some similarities with the former monsoon stage, with the main moisture source being found in the west Pacific Ocean, East China, the South China Sea, and the Indian Ocean. It is interesting to note that the Indian Ocean channel is the main moisture pathway, but the Indian Ocean does not constitute the main moisture source. In fact, as shown in Fig. 5c, the pathway from the Indian Ocean goes through the Indian Peninsula and the Indochina Peninsula, and a significant part of moisture from the Indian Ocean is lost along the trajectories. By consequence, in the spatial distribution of CDF (Fig. 5d), the Indian Ocean is not the most important moisture source, with a contribution density to precipitation from only about  $1.0 \times 10^{-5}$  to  $1.0 \times 10^{-4}$ .

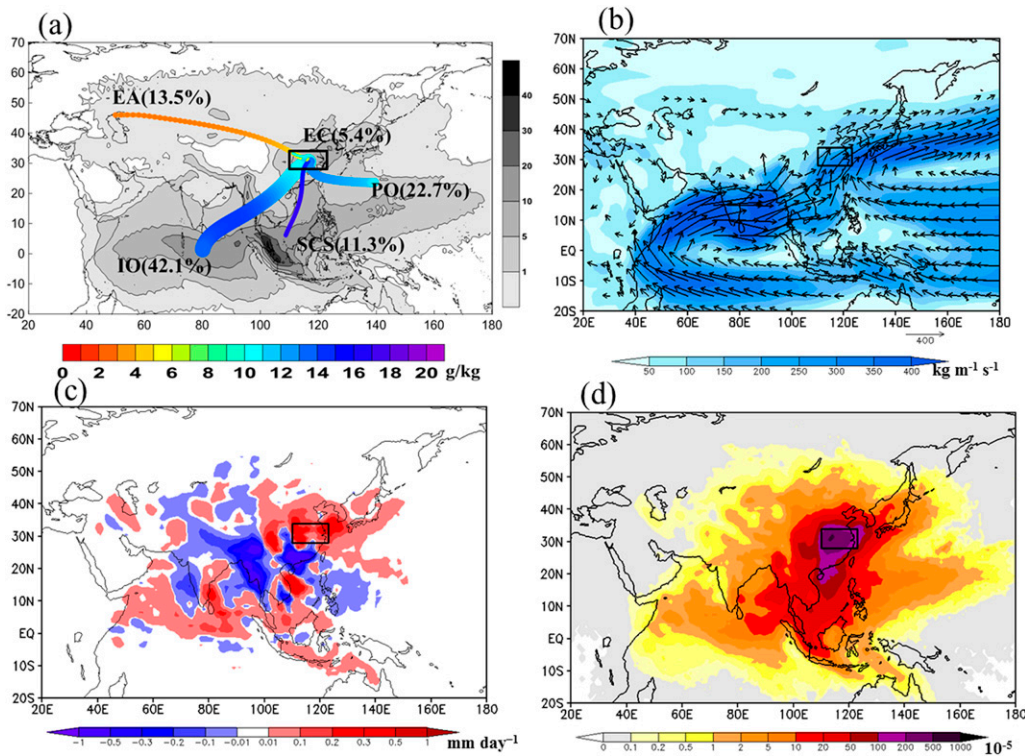


FIG. 5. As in Fig. 3, but for the phase of the monsoon (mei-yu) in the Yangtze–Huaihe River basin.

The maximum of the contribution density, larger than  $1.0 \times 10^{-3}$ , is in the Yangtze–Huaihe River basin itself and in South China. Compared to the monsoon in South China, the mei-yu period shows the CDF decreasing in the south and increasing in the north. The CDF in the Indian Ocean and South China Sea decreases, but the region of CDF exceeding  $1.0 \times 10^{-5}$  extends to  $50^{\circ}\text{N}$ .

For the mei-yu stage of EASM in the Yangtze–Huaihe River basin, the most important moisture channel is still that from the Indian Ocean, which comprises 43.4% of the trajectories. But it has great moisture loss along the trajectories, so the moisture contribution for the precipitation is relatively small. The most important moisture contribution region is the Yangtze–Huaihe River basin and South China.

#### d. Terminal stage of monsoon in North China

The North China rainy season is the terminal stage of EASM. As the monsoon moves to North China, the rainy belt also shifts to North China and can stay for a few weeks. During the monsoon terminal stage in North China, the most important moisture transport paths change from the IO to midlatitude westerlies and to the PO (Fig. 6a), the proportions for these two channels being 30.3% and 26.8%, respectively. As

shown in Fig. 6b, the IO channel, the SCS channel, and the PO channel move northward to North China, affecting the local rainfall. Midlatitude westerlies also influence the rain belt. It should be noticed that, although the number of trajectories in the midlatitude westerlies is the biggest, the specific humidity of this channel is small, so the vertically integrated water vapor transport in this channel is relatively small. Our results confirm those of Jiang et al. (2017), who showed that Eurasia has the maximum parcels and the Pacific Ocean has the second largest number of parcels during the rainy season in North China.

Figure 6c is the spatial distribution of  $E - P$  for the terminal stage of EASM in North China. The main moisture source regions for the rainfall in North China are the eastern coastal areas of China, the northern part of the South China Sea, and the Yangtze–Huaihe River basin. The main moisture sink regions are North China, South China, and the Indochina Peninsula. The spatial distribution of CDF to precipitation in North China indicates that the maximum value is still near the target area, and the average contribution density exceeds  $5.0 \times 10^{-3}$ . The CDF in the south is further reduced; only the South China Sea and small areas east of Taiwan show CDF values higher than  $1.0 \times 10^{-4}$ . Meanwhile, the CDF in the north is significantly increased. The region contour

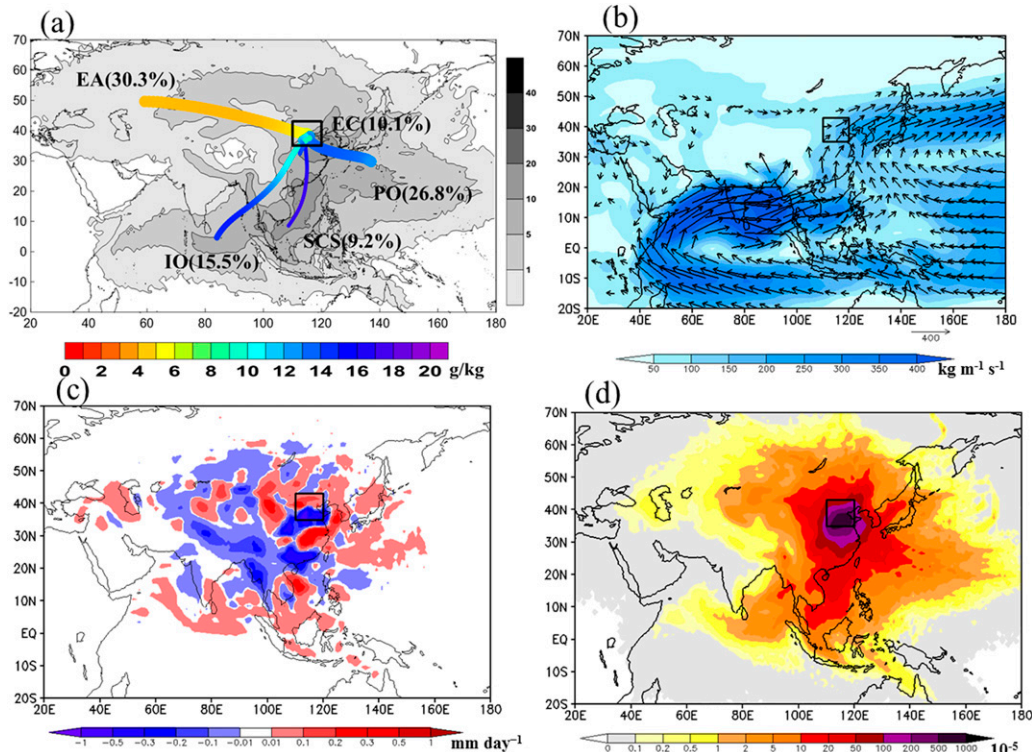


FIG. 6. As in Fig. 3, but for the terminal stage of the monsoon in North China.

$1.0 \times 10^{-5}$  reaches to Balkhash Lake in the west and  $60^{\circ}\text{N}$  in the north. On the whole, the main moisture transport channels during the terminal stage of monsoon in North China are those from the midlatitude westerlies and the west Pacific Ocean, with trajectories rates of 30.3% and 26.8%, respectively. But there is low specific humidity from the westerlies channel, so the westerlies channel has little influence for the monsoon in North China. The most important moisture sources are from East China.

#### e. Moisture transport evolution during the northward propagation of the EASM

From what shown above, it is clear that, accompanying the northward propagation of the EASM, the main water vapor channel experiences profound changes. It is sourced in the west Pacific Ocean (PO) for the premonsoon in South China (SC). It changes then to the Indian Ocean (IO) when the monsoon sets up in SC and in the Yangtze–Huaihe River basin. Finally the main water vapor channel is back to PO for the terminal stage of monsoon in North China. As shown in Fig. 7, the proportion of trajectories shows quite distinct behaviors for their seasonal evolution. The two channels from south and southwest (SCS channel and IO channel) increase first, and then decrease with the northward shift of the rain belt. In contrast, the water vapor

channels from the midlatitude westerly, the west Pacific Ocean, and the local moisture recycling show opposite characteristics, with an initial decrease followed by an increase.

Not only do the water vapor channels change profoundly following the seasonal course of the summer monsoon, but also the spatial distribution of water vapor contribution leading to rainfall shows strong changes from one period to another. Figure 8 shows difference maps of CDF between two sequential stages. From the premonsoon to the onset of monsoon in South China, the moisture contribution from the Indian Ocean and the southern part of the South China Sea has an obvious increase. Meanwhile, there are decreases of CDF in the northern part of the South China Sea and in the west Pacific Ocean. This situation is largely expected since the onset of the monsoon in India and in South China implies much more water vapor coming from the southwest. A large decreasing zone covering the Bay of Bengal, South China, and the adjacent South China Sea reflects strong monsoon rainfalls in these areas. It is to be noted that there is a zone of increasing CDF in the northwest area of our target region, certainly related to the special topography in the lee side of the Tibetan Plateau.

When the monsoon rain belt reaches the Yangtze–Huaihe River basin, we observe an opposite situation as

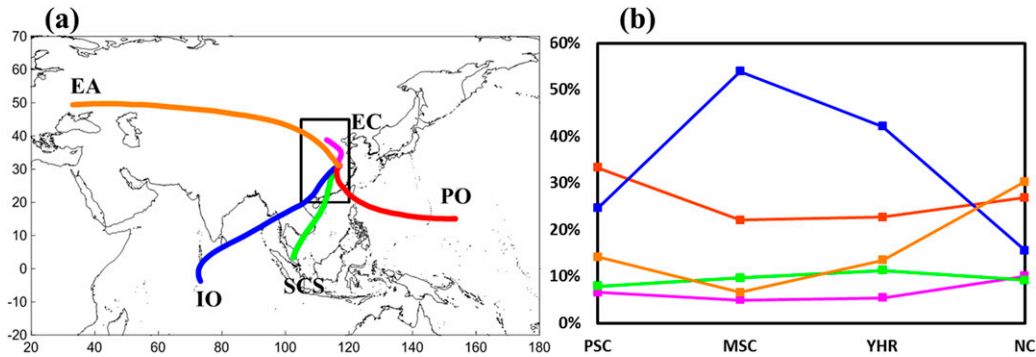


FIG. 7. (a) Schematic showing the five main moisture channels from East China (EC) itself, the west Pacific Ocean (WPO), the South China Sea (SCS), the Indian Ocean (IO), and the Eurasian westerly (EA), that affect precipitation in East China. (b) Proportions of trajectories from different channels in function of the four major stages of the East Asian summer monsoon: premonsoon in South China (PSC), monsoon in South China (MSC), mei-yu in the Yangtze–Huaihe River basin (YHR), and terminal stage of monsoon in North China (NC).

shown in Fig. 8b. There is a clear dipole with decreasing contribution from the south and increasing contribution from the north. The demarcation line is located around 25°–30°N. As we mentioned earlier, the northward shift of the research region reflects the seasonal migration of the summer monsoon, which induces a systematic northward shift of the water vapor contribution. This phenomenon is also visible in Fig. 8c, which displays the changes of CDF when the monsoon shifts from the Yangtze–Huaihe River basin to its terminal stage in North China. The water vapor from the north is more important and that from the south is less important. It should be noticed that the moisture contribution from the Pacific Ocean is larger, showing a more important role played by the west Pacific Ocean.

*f. Contributions from different source regions*

From what was described previously, we can see that our Lagrangian trajectories can be quantitatively used to assess the intensity of moisture transport channels

and determine the main pathway in each stage of the monsoonal northward propagation. The evaporation-minus-precipitation diagnosis considering the absorption and release of moisture along the trajectories can further determine the source characteristics of water vapor. Finally, the improved areal source–receptor attribution method allows us to quantify the moisture contribution of each source for the precipitation in the target region. With the northward propagation of EASM, significant changes take place in water vapor channels, including moisture sources and water vapor contributions to rainfall. In this section, we study further the properties of CDF, which is a new measure with powerful diagnostic abilities. We want to focus on its dynamic evolution in function with regard to the monsoon northward propagation.

To be consistent with the above-shown moisture transport channel, we use the same five moisture source regions: 1) East China (EC), 2) the west Pacific Ocean (PO), 3) the South China Sea (SCS), 4) the Indian Ocean (IO)

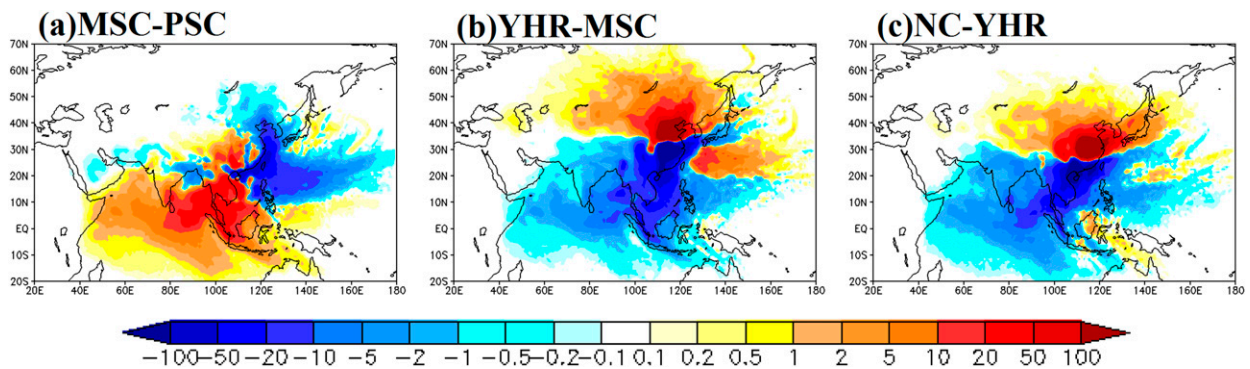


FIG. 8. Sequential changes of the water vapor CDF among the four stages of the summer monsoon course: (a) stage 2 – stage 1, (b) stage 3 – stage 2, and (c) stage 4 – stage 3 ( $10^{-5}$ ; areas of  $1^\circ \times 1^\circ$  latitude/longitude).

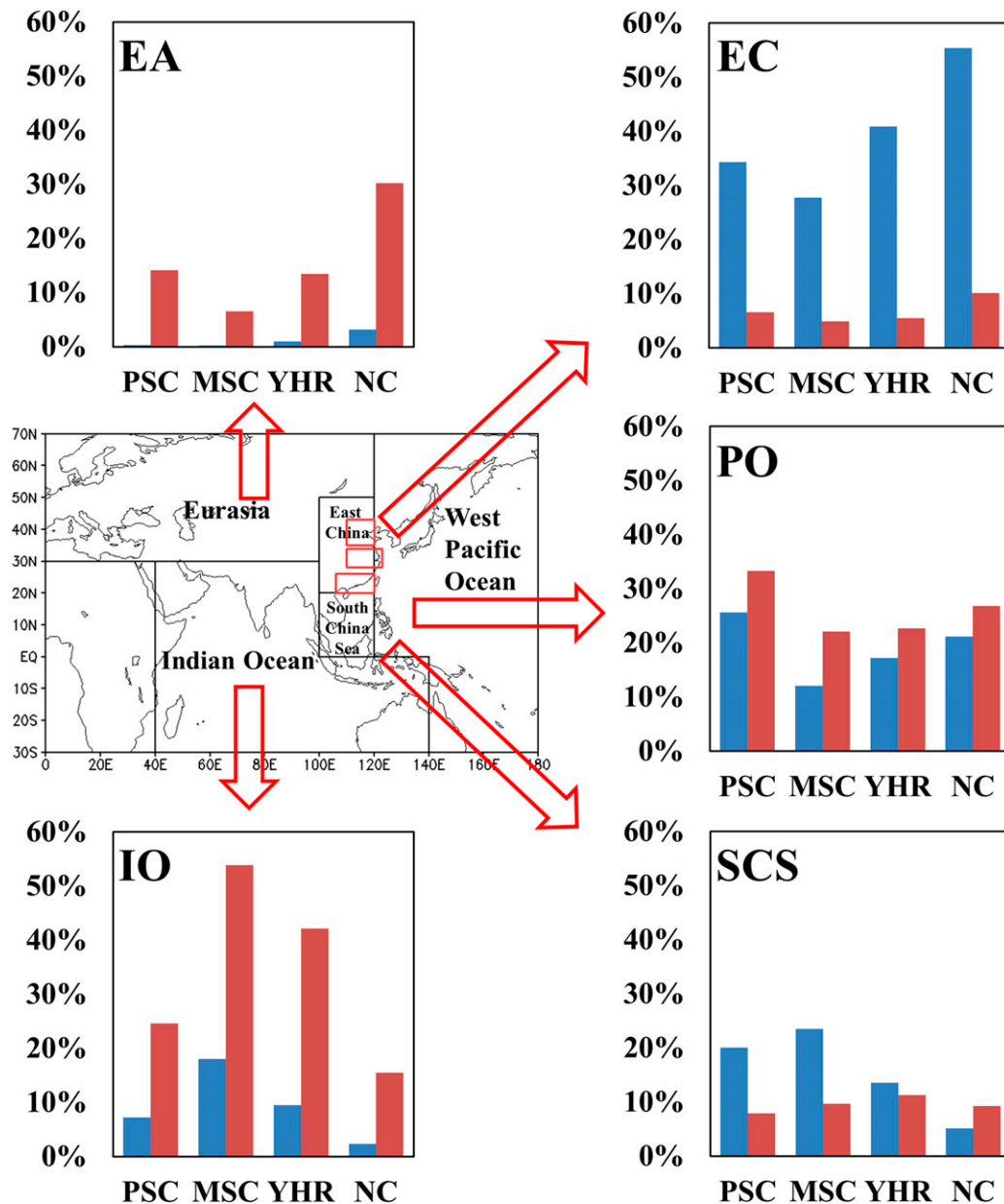


FIG. 9. Bar charts showing the proportion of trajectories (red bars; %) and moisture contributions (blue bars; %) leading to precipitation in different stages of the summer monsoon (PSC: premonsoon in South China; MSC: monsoon in South China; YHR: monsoon or mei-yu in the Yangtze–Huaihe River basin; NC: terminal monsoon in North China). Background map shows the division of geographic sectors (black boxes: East China, South China Sea, Indian Ocean, west Pacific Ocean, and Eurasia) used to account the trajectories and moisture contributions.

and 5) Eurasia (EA) (Fig. 9, background map). We can now calculate the moisture contribution to precipitation for each of these source regions by just integrating the contribution density function for each region. It is also relevant to compare such regional contributions to the intensity of each moisture transport channel.

As shown in Fig. 9, the moisture contribution from East China to regional precipitation is very high for all

the four stages of the summer monsoon. This regional moisture contribution is well above the proportion of trajectories. In fact, all proportions of trajectories are under 10%, but the moisture contributions are mostly over 30%. This result clearly indicates that more than 30% of the moisture for precipitation in East China originated from local evaporations. The local water recycling plays an important role for precipitation in each

stage of the rainy season. Obviously, this kind of local evaporation is closely related to the hydrological conditions and vegetation behaviors of the underlying surface. In fact, it is closely related to early precipitation. Previous studies have also shown that soil moisture is an important factor for monthly and seasonal forecasting (Walker and Rowntree 1977; Tuttle and Salvucci 2016). Zuo and Zhang (2007) already pointed out that spring precipitation and soil moisture in East China exert an important effect on summer precipitation. It is remarkable that, after the onset of SCS summer monsoon, soil moisture accumulation in East China due to earlier precipitation enhances local evaporation and then precipitation. This is especially true for the terminal stage of monsoon in North China with a regional moisture contribution up to 55%, reflecting that local water vapor recycling and precipitation in the early rainy season play a very important role in the regional monsoon strength. In general, evaporation in East China plays an important role for the rainfall in the EASM.

The PO is also an important moisture source region contributing to precipitation in East China. The regional contributions from the PO are all larger than 10%. It is the highest (25%) for the premonsoon in South China. The second largest contribution (>20%) is found for the terminal stage of monsoon in North China.

The moisture contribution from the SCS shows a big difference between the rainfall stage in South China and other two stages in the Yangtze River valley and in North China during the monsoon seasonal course. In South China, no matter whether before or after the onset of the SCS summer monsoon, the moisture contributions from SCS are both larger than 20%, which constitutes an important moisture source. But when the monsoon goes to the Yangtze River basin and farther to North China, this moisture contribution diminishes rapidly, until the contribution is only 5.1% in the terminal stage of monsoon in North China.

For the Indian Ocean, if we examine the proportion of trajectories, we can see that the IO water vapor transport channel is an important one for the whole monsoon course. This is in agreement with our general belief. In particular, for rainfall period in South China and the mei-yu in the Yangtze–Huaihe River valley, we can account about half of the trajectories. However, if we examine the moisture contribution to the actual precipitation, a different image appears. The contribution from IO is actually quite small. For the four sub-periods of the monsoon seasonal course, it is only 7.2%, 18.0%, 9.5%, and 2.4%, respectively. The main reason is that the pathway of the IO channel goes through the Indian Peninsula and the Indochina Peninsula which are important moisture sink regions to the rainfall in target

region. Moisture is thus lost along the trajectories, which induces a low contribution from the Indian Ocean for precipitation in East China.

Eurasian land is another region for which the “true” moisture contribution rates are all lower than the proportions of accounted trajectories. As shown in Fig. 8, the trajectory rates are all larger than 10% except when the monsoon is in South China, but enhanced when the monsoon reached North China. For the latter case, the proportion of trajectories from midlatitude westerlies reaches its peak value of 30.2%. In terms of moisture contribution to precipitation, all contributions from EA are smaller than 3.5%. The main reason is that the specific humidity of air parcels from EA is small (Fig. 3a). Therefore, the impact on precipitation of EASM is also small.

In summary, with the northward migration of EASM during its seasonal course, the moisture transport channels and moisture source regions show continuous and significant changes. The main water vapor channel is first from the PO for the premonsoon in South China. It is then from the IO for the starting monsoon in South China and mei-yu in the Yangtze–Huaihe River basin. Finally, it returns to the PO in the terminal stage of monsoon in North China. Based on the evaporation-minus-precipitation diagnosis and the areal source–receptor attribution method, the main moisture source during the premonsoon in South China is the PO and EC and the contribution rates are 34.3% and 27.7%, respectively. After the onset of the South China Sea summer monsoon, EC and SCS are the most important moisture sources in this period, their contribution rates being both larger than 23%. During mei-yu in the Yangtze–Huaihe River basin and terminal stage of monsoon in North China, the moisture of this period mainly comes from EC, the contribution rate reaching to 40.9% and 55.3%, respectively. Furthermore, our results on water vapor channels are consistent with published literature, such as Lin et al. (2014), Chen and Luo (2018), Zuo et al. (2009), and Jiang et al. (2017). But it is clear that the main moisture actually contributing to EASM precipitation does not necessarily come from the strongest water vapor pathways. For example, the trajectory proportions for the IO are larger than 25% especially in the stage of monsoon in South China (53%), but the moisture contributions are generally smaller than 10%. This is mainly due to the fact that a large amount of water vapor is actually lost in the transport pathways through important moisture sink areas such as the Indian Peninsula and Indochina Peninsula. On the contrary, local water vapor recycling inside EC plays an important role for the regional precipitation, with contributions mostly over 30%, although the trajectory

proportions for EC are all under 10%. The contribution rate can even exceed 55% for the terminal stage of monsoon in North China.

Our results seem qualitatively in agreement with Sun and Wang (2015), who emphasized the role of land evaporation in precipitation falling in the Yangtze–Huaihe River basin and in North China. Similar conclusions are also reported in Drumond et al. (2011a) for precipitation in different regions of China. One can also mention the work of Drumond et al. (2011b) investigating precipitation in the Mediterranean area. It was convincingly shown that local sources provide moisture for the eastern Mediterranean and western North Africa. However, if we quantitatively compare our results to those reported in Sun and Wang (2015), our results seem to give larger weights on evaporation along the trajectories. This is certainly due to the fact that we incorporated a rule of boundary layer water vapor source in our calculations.

#### 4. Conclusions and discussion

In this paper, we used the HYSPLIT platform to calculate Lagrangian trajectories of air parcels that reach East China during the northward propagation of the East Asian summer monsoon. Our study, with NCEP–NCAR reanalysis data as driving conditions, covers a long period from 1961 to 2010 to ensure the significance of results. In the online supplemental material, we explored the sensitivity of our results to two other datasets and to the use of a second Lagrangian trajectory model, FLEXPART. The difference is estimated below 5% among different datasets and below 10% between the two Lagrangian models. To fully explore the Lagrangian trajectories, we calculate the mean moisture trajectories to get the main moisture channel. Since water vapor is not a conservative tracer following the trajectories, we also elaborated the evaporation-minus-precipitation diagnosis and the areal source–receptor attribution of water vapor contribution. We can thus obtain a robust picture for the water vapor transport, including paths, moisture sources, and moisture contribution from different regions to precipitation in EASM. The main findings are summarized below.

Four main water vapor channels and their contribution have significant changes while the rain belt in East China propagates from south to north. These water vapor channels are from the west Pacific Ocean (PO), the Indian Ocean (IO), the South China Sea (SCS), and the midlatitude westerlies, respectively. And local transportation also plays an important role in each rainy season. In the premonsoon stage with rainfall in South China, the most important moisture

transport channels are from the PO and IO, the proportion of the trajectories being 33.3% and 24.6% respectively, consistent with our general expectation. But the main moisture sources are from East China and the PO, with moisture contribution rates at 34.3% and 25.7% respectively, highlighting the role of local evaporation for precipitation. After the onset of the SCS summer monsoon, but when the monsoon rain belt is still in South China, the IO channel strengthens, with the trajectory proportion increasing to 53.9%. This reflects the onset of the Indian monsoon, which enters into the South China Sea. Despite the Indian monsoon strengthening, EC and the SCS are, however, the most important moisture sources in this period, their contribution rates to precipitation being both larger than 23%. For mei-yu in the Yangtze–Huaihe River basin, the IO channel is still the most important water vapor channel, which includes 42.1% of all the trajectories. But the contribution rate from East China to precipitation is the highest (40.9%). East China becomes the most important moisture source region. When the monsoon is in its terminal stage in North China, the most important moisture channels are the midlatitude westerlies channel and the PO channel, their trajectory proportions being 30.3% and 26.8%, respectively, and the local water vapor recycling in East China has the greatest contribution to rainfall in North China during this stage, with its contribution rate exceeding 55%.

It is worth emphasizing that the main moisture for the EASM precipitation does not necessarily come from the strongest water vapor pathways. For example, the trajectory proportions for the IO are all larger than 25% (exceeding 53% in the stage of monsoon in South China), but moisture contributions to rainfall are always smaller than 10%. This counterintuitive result is in fact quite logical, since a large amount of water vapor is lost in the transport pathways crossing important moisture sink areas such as the Indian Peninsula and Indochina Peninsula. On the contrary, local water vapor recycling inside East China plays an important role for the regional precipitation, with contributions mostly over 30%, especially in the terminal stage of monsoon in North China when the contribution rate can even exceed 55%, although the trajectory proportions for East China are all under 10%.

Finally, we can see that our analysis based on Lagrangian trajectories provides very useful information on water vapor transport, its source–sink regions, and its contributions to rainfall. Results are generally in agreement with Eulerian diagnosis of water vapor transport. The focus of this study was on precipitation in East China during the northward migration course of the regional summer monsoon. We examined only

climatological fields. It is necessary to extend the current study to investigating interannual and interdecadal variations of moisture transport.

*Acknowledgments.* Constructive comments from three anonymous reviewers were very helpful to improve an earlier version of this paper. We thank Dr. Sun Bo for his great help on technology guidance. We acknowledge the National Climate Center (NCC) of China (<http://ncc.cma.gov.cn>) for the observations and NOAA, the Air Resources Laboratory (ARL), from ARL's archives ([http://ready.arl.noaa.gov/gbl\\_reanalysis.php](http://ready.arl.noaa.gov/gbl_reanalysis.php)) for NCEP–NCAR reanalysis data. This work is supported by the National Natural Science Foundation of China (41675081), and the National Key Research and Development Program of China (Grant 2016YFA0600402). Zhengyu Liu is partly supported by the U.S. NSF P2C2. Laurent Li is partly supported by the French ANR project China-Trend-Stream and the National Key Research and Development Program of China (Grant 2018YFC1507704).

#### REFERENCES

- Bertò, A., A. Buzzi, and D. Zardi, 2004: Back-tracking water vapour contributing to a precipitation event over Trentino: A case study. *Meteor. Z.*, **13**, 189–200, <https://doi.org/10.1127/0941-2948/2004/0013-0189>.
- Bottyán, E., G. Czuppon, K. Kármán, T. Weidinger, and L. Haszpra, 2014: Moisture source diagnostic for Hungary based on trajectory analysis and stable isotopic composition of precipitation. *Proc. 2014 EGU General Assembly*, Vienna, Austria, EGU, vol. **16**, p. 2014.
- Brubaker, K. L., P. A. Dirmeyer, A. Sudradjat, B. S. Levy, and F. Bernal, 2001: A 36-yr climatological description of the evaporative of warm-season precipitation in the Mississippi river basin. *J. Hydrometeor.*, **2**, 537–557, [https://doi.org/10.1175/1525-7541\(2001\)002<0537:AYCDOT>2.0.CO;2](https://doi.org/10.1175/1525-7541(2001)002<0537:AYCDOT>2.0.CO;2).
- Chang, C. P., 2004: *East Asian Monsoon*. World Scientific, 564 pp.
- Chen, B., X. Xu, and T. Zhao, 2013: Main moisture sources affecting lower Yangtze River Basin in boreal summers during 2004–2009. *Int. J. Climatol.*, **33**, 1035–1046, <https://doi.org/10.1002/joc.3495>.
- Chen, L., and Coauthors, 1991: *East Asia Monsoon* (in Chinese). China Meteorological Press, 362 pp.
- Chen, Y., and Y. Luo, 2018: Analysis of paths and sources of moisture for the South China rainfall during the presummer rainy season of 1979–2014. *J. Meteor. Res.*, **32**, 744–757, <https://doi.org/10.1007/s13351-018-8069-7>.
- Chi, Y., J. He, and W. Wu, 2005: Features analysis of the different precipitation periods in the pre-flood season in South China. *J. Nanjing Inst. Meteor.*, **28**, 163–171.
- Chu, Q., Q. Wang, and G. Feng, 2017: Determination of the major moisture sources of cumulative effect of torrential rain events during the pre-flood season over South China using a Lagrangian particle model. *J. Geophys. Res.*, **122**, 8369–8382, <https://doi.org/10.1002/2016JD026426>.
- Diem, J. E., and D. P. Brown, 2006: Tropospheric moisture and monsoonal rainfall over the southwestern United States. *J. Geophys. Res.*, **111**, D16112, <https://doi.org/10.1029/2005JD006836>.
- Ding, Y., Z. Wang, and Y. Sun, 2008: Inter-decadal variation of the summer precipitation in East China and its association with decreasing Asian summer monsoon. Part I: Observed evidences. *Int. J. Climatol.*, **28**, 1139–1161, <https://doi.org/10.1002/joc.1615>.
- Dirmeyer, P. A., K. L. Brubaker, and T. DelSole, 2009: Import and export of atmospheric water vapor between nations. *J. Hydrol.*, **365**, 11–22, <https://doi.org/10.1016/j.jhydrol.2008.11.016>.
- Dominguez, F., P. Kumar, X. Liang, and M. Ting, 2006: Impact of atmospheric moisture storage on precipitation recycling. *J. Climate*, **19**, 1513–1530, <https://doi.org/10.1175/JCLI3691.1>.
- , G. Miguez-Macho, and H. Hu, 2016: WRF with water vapor tracers: A study of moisture sources for the North American monsoon. *J. Hydrometeor.*, **17**, 1915–1927, <https://doi.org/10.1175/JHM-D-15-0221.1>.
- Draxler, R. R., and G. Hess, 1998: An overview of the HYSPLIT\_4 modelling system for trajectories. *Aust. Meteor. Mag.*, **47**, 295–308.
- Drumond, A., R. Nieto, and L. Gimeno, 2011a: Sources of moisture for China and their variations during drier and wetter conditions in 2000–2004: A Lagrangian approach. *Climate Res.*, **50**, 215–225, <https://doi.org/10.3354/cr01043>.
- , —, E. Hernandez, and L. Gimeno, 2011b: A Lagrangian analysis of the variation in moisture sources related to drier and wetter conditions in regions around the Mediterranean Basin. *Nat. Hazards Earth Syst. Sci.*, **11**, 2307–2320, <https://doi.org/10.5194/nhess-11-2307-2011>.
- Eiras-Barca, J., F. Dominguez, H. Hu, D. Garaboa-Paz, and G. Miguez-Macho, 2017: Evaluation of the moisture sources in two extreme landfalling atmospheric river events using an Eulerian WRF tracers tool. *Earth Syst. Dyn.*, **8**, 1247–1261, <https://doi.org/10.5194/esd-8-1247-2017>.
- Gimeno, L., A. Drumond, R. Nieto, R. M. Trigo, and A. Stohl, 2010: On the origin of continental precipitation. *Geophys. Res. Lett.*, **37**, L13804, <https://doi.org/10.1029/2010GL043712>.
- Huang, R., Z. Zhang, G. Huang, and B. Ren, 1998: Characteristics of the water vapor transport in East Asian monsoon region and its difference from that in South Asian monsoon region in summer. *Chin. J. Atmos. Sci.*, **22**, 469–479.
- Huang, W., X. He, Z. Yang, T. Qiu, J. S. Wright, B. Wang, and D. Lin, 2018: Moisture sources for wintertime extreme precipitation events over South China during 1979–2013. *J. Geophys. Res.*, **123**, 6690–6712, <https://doi.org/10.1029/2018JD028485>.
- Insua-Costa, D., and G. Miguez-Macho, 2018: A new moisture tagging capability in the Weather Research and Forecasting model: Formulation, validation and application to the 2014 Great Lake–effect snowstorm. *Earth Syst. Dyn.*, **9**, 167–185, <https://doi.org/10.5194/esd-9-167-2018>.
- Jiang, X., Y. Li, and X. Wang, 2009: Water vapor transport over China and its relationship with drought and flood in Yangtze River Basin. *J. Geogr. Sci.*, **19**, 153–163, <https://doi.org/10.1007/s11442-009-0153-6>.
- Jiang, Z., J. He, J. Li, J. Yang, and J. Wang, 2006: Northerly advancement characteristics of the East Asian summer monsoon with its interdecadal variations (in Chinese). *Acta Geogr. Sin.*, **61**, 675–686.
- , W. Ren, Z. Liu, and H. Yang, 2013: Analysis of water vapor transport characteristics during the Meiyu over the Yangtze-Huaihe River valley using the Lagrangian method (in Chinese). *Acta Meteor. Sin.*, **271**, 295–304.

- , S. Jiang, Y. Shi, Z. Liu, W. Li, and L. Li, 2017: Impact of moisture source variation on decadal-scale changes of precipitation in North China from 1951 to 2010. *J. Geophys. Res.*, **122**, 600–613, <https://doi.org/10.1002/2016JD025795>.
- Lin, A., D. Gu, B. Zheng, C. Li, and J. Zhang, 2014: Anomalous transport of water vapor for sustained torrential rain and its variation (in Chinese). *J. Trop. Meteor.*, **30**, 1001–1010.
- Martius, O., and Coauthors, 2013: The role of upper-level dynamics and surface processes for Pakistan flood of July 2010. *Quart. J. Roy. Meteor. Soc.*, **139**, 1780–1797, <https://doi.org/10.1002/qj.2082>.
- NOAA ARL, 2011: HYSPLIT (HYbrid Single-Particle Lagrangian Integrated Trajectory). National Oceanic and Atmospheric Administration, Air Resources Laboratory, <https://ready.arl.noaa.gov/HYSPLIT.php>.
- Perry, L. B., C. E. Konrad, and T. W. Schmidlin, 2007: Antecedent upstream air trajectories associated with northwest flow snowfall in the southern Appalachians. *Wea. Forecasting*, **22**, 334–352, <https://doi.org/10.1175/WAF978.1>.
- Shen, R., and Coauthors, 1982: Low latitude circulation variation in the high and low level of convective layer and precipitation during the pre-rainy season in South China (in Chinese). *Proceedings of the National Conference on Tropical Summer Monsoon*. Yunnan People's Publishing House, 10–21.
- Shi, Y., X. J. Gao, Y. G. Wang, and F. Giorgi, 2009: Simulation and projection of monsoon rainfall and rain patterns over eastern China under global warming by RegCM3. *Atmos. Oceanic Sci. Lett.*, **2**, 308–313, <https://doi.org/10.1080/16742834.2009.11446816q>.
- Sodemann, H., and A. Stohl, 2009: Asymmetries in the moisture origin of Antarctic precipitation. *Geophys. Res. Lett.*, **36**, L22803, <https://doi.org/10.1029/2009GL040242>.
- , and E. Zuber, 2010: Seasonal and inter-annual variability of the moisture sources for Alpine precipitation during 1995–2002. *Int. J. Climatol.*, **30**, 947–961, <https://doi.org/10.1002/JOC.1932>.
- , C. Schwierz, and H. Wernli, 2008: Interannual variability of Greenland winter precipitation sources: Lagrangian moisture diagnostic and North Atlantic Oscillation influence. *J. Geophys. Res.*, **113**, D03107, <https://doi.org/10.1029/2007JD008503>.
- Stohl, A., and P. James, 2004: A Lagrangian analysis of the atmospheric branch of the global water cycle. Part I: Method description, validation, and demonstration for the August 2002 flooding in central Europe. *J. Hydrometeorol.*, **5**, 656–678, [https://doi.org/10.1175/1525-7541\(2004\)005<0656:ALAOTA>2.0.CO;2](https://doi.org/10.1175/1525-7541(2004)005<0656:ALAOTA>2.0.CO;2).
- , and —, 2005: A Lagrangian analysis of the atmospheric branch of the global water cycle. Part II: Moisture transports between Earth's ocean basins and river catchments. *J. Hydrometeorol.*, **6**, 961–984, <https://doi.org/10.1175/JHM470.1>.
- Sun, B., and H. Wang, 2014: Moisture sources of semi-arid grassland in China using the Lagrangian Particle Model FLEX-PART. *J. Climate*, **27**, 2457–2474, <https://doi.org/10.1175/JCLI-D-13-00517.1>.
- , and —, 2015: Analysis of the major atmospheric moisture sources affecting three sub-regions of east China. *Int. J. Climatol.*, **35**, 2243–2257, <https://doi.org/10.1002/joc.4145>.
- , Y. L. Zhu, and H. J. Wang, 2011: The recent interdecadal and interannual variation of water vapor transport over eastern China. *Adv. Atmos. Sci.*, **28**, 1039–1048, <https://doi.org/10.1007/s00376-010-0093-1>.
- Tuttle, S., and G. Salvucci, 2016: Empirical evidence of contrasting soil moisture–precipitation feedbacks across the United States. *Science*, **352**, 825–828, <https://doi.org/10.1126/science.aaa7185>.
- Walker, J., and P. R. Rowntree, 1977: The effect of soil moisture on circulation and rainfall in a tropical model. *Quart. J. Roy. Meteor. Soc.*, **103**, 29–46, <https://doi.org/10.1002/qj.49710343503>.
- Wang, B., 2006: *The Asian Monsoon*. Springer Science & Business Media, 787 pp.
- , H. Lin, Y. Zhang, and M. M. Lu, 2004: Definition of South China Sea monsoon onset and commencement of the East Asia summer monsoon. *J. Climate*, **17**, 699–710, <https://doi.org/10.1175/2932.1>.
- Wei, J., P. A. Dirmeyer, M. G. Bosilovich, and R. Wu, 2012: Water vapor sources for Yangtze River Valley rainfall: Climatology, variability, and implications for rainfall forecasting. *J. Geophys. Res.*, **117**, D05126, <https://doi.org/10.1029/2011JD016902>.
- Xie, K., and X. Ren, 2008: Climatological characteristics of atmospheric water vapor transport and its relation with rainfall over north China in summer (in Chinese). *Sci. Meteor. Sin.*, **28**, 5508–5514.
- Xu, X., L. Chen, X. Wang, Q. Miao, and S. Tao, 2004: Moisture transport source/sink structure of the meiyu rain belt along the Yangtze River valley. *Chin. Sci. Bull.*, **49**, 181–188.
- , X. Shi, Y. Wang, S. Peng, and X. Shi, 2008: Data analysis and numerical simulation of moisture source and transport associated with summer precipitation in the Yangtze River valley over China. *Meteor. Atmos. Phys.*, **100**, 217–231, <https://doi.org/10.1007/s00703-008-0305-8>.
- Zhou, T., and R. Yu, 2005: Atmospheric water vapor transport associated with typical anomalous summer rainfall patterns in China. *J. Geophys. Res.*, **110**, D08104, <https://doi.org/10.1029/2004JD005413>.
- Zhu, Y., H. J. Wang, W. Zhou, and J. G. Ma, 2011: Recent changes in the summer precipitation pattern in East China and the background circulation. *Climate Dyn.*, **36**, 1463–1473, <https://doi.org/10.1007/s00382-010-0852-9>.
- Zuo, J., H. Ren, W. Li, P. Zhang, and M. Yang, 2009: Intra-seasonal characteristics of water vapor transport associated with low-frequency rainfall regimes over southern China in summer. *Chin. J. Geophys.*, **52**, 922–935, <https://doi.org/10.1002/cjg2.1417>.
- Zuo, Z., and R. Zhang, 2007: The spring soil moisture and the summer rainfall in eastern China. *Chin. Sci. Bull.*, **52**, 3310–3312, <https://doi.org/10.1007/s11434-007-0442-3>.